

# Toward structural LES modeling with high-order spectral difference schemes

Guido Lodato\*, Patrice Castonguay† and Antony Jameson‡

*Department of Aeronautics and Astronautics, Stanford University, Stanford, CA 94305, USA*

The combination of the high-order unstructured spectral difference spatial discretization scheme with sub-grid scale modeling for large-eddy simulation was investigated with particular focus on the consistent implementation of a structural mixed model based on the scale similarity hypothesis. The difficult task of deriving a consistent formulation for the discrete filter within hexahedral elements of arbitrary order led to the development of a new class of three-dimensional constrained discrete filters. Results from computations of turbulent channel flow at  $Re_\tau = 180$  and 395 and flow past a confined circular cylinder at  $Re_D = 2580$  were compared against direct numerical simulation and particle image velocimetry measurements, respectively. The numerical experiments suggest that the results are sensitive to the use of an sub-grid scale closure, even when a high-order numerical scheme is used, especially when the grid resolution is kept relatively low. The use of the similarity mixed formulation proved to be particularly accurate in reproducing sub-grid scale interactions, confirming that its well-known potential can be realized in conjunction with state-of-the-art high-order numerical schemes.

## I. Introduction

Notwithstanding the considerable effort which has been devoted to the development of accurate and relatively reliable Sub-Grid Scale (SGS) models for Large-Eddy Simulation (LES), the underlying numerical methods, which are available within the framework of industrial computational fluid dynamics applications generally rely upon highly dissipative schemes. The inherent numerical dissipation introduced by such numerical schemes limits their ability to correctly represent the whole spectrum resolved in LES.

Hence it is necessary to combine high order numerical schemes with advanced SGS modeling techniques in order for LES to become a valuable and reliable tool for fundamental flow physics and industrial applications. Unfortunately, most of the available high-order numerical schemes are designed to be used on cartesian or very smooth structured curvilinear meshes and therefore they are inadequate to simulate turbulent flows over complex geometries. In the current work, a high-order unstructured solver is combined with an explicit filtering LES method, thus allowing highly accurate turbulent flow computations on realistic geometries that were previously only possible with low-order schemes.

High-order numerical schemes for solving the compressible Navier-Stokes equations on unstructured grids have been widely studied during the last decade. By far the most mature and widely used of these schemes are based on the Discontinuous Galerkin (DG) method.<sup>1,2</sup> However, several alternative high-order methods have been recently proposed, including Spectral Difference (SD) type schemes,<sup>3-9</sup> which potentially offer increased efficiency compared with DG methods (as well as being simpler to implement). The SD method has been successfully applied to viscous compressible flows with shocks,<sup>10</sup> implicit LES of turbulent channel flow,<sup>11</sup> and flow around circular cylinders,<sup>12,13</sup> as well as, transitional flows over an SD7003 airfoil.<sup>14</sup> The combination of the SD method with SGS modeling techniques for explicit LES, on the other hand, has not been widely studied. Parsani et al.<sup>15</sup> obtained encouraging results using the Wall-Adapting Local Eddy-viscosity (WALE) model<sup>16</sup> but their analysis was restricted to two-dimensional flows. A three-dimensional computation of turbulent flow in a muffler at  $Re = 46\,650$  was also reported.<sup>17</sup>

\*Postdoctoral Research Fellow, Aeronautics and Astronautics Department, Stanford University, Member AIAA.

†PhD Candidate, Aeronautics and Astronautics Department, Stanford University, Member AIAA.

‡Thomas V Jones Professor, Aeronautics and Astronautics Department, Stanford University, Fellow AIAA.

Copyright © 2012 by G. Lodato, P. Castonguay and A. Jameson. Published by the American Institute of Aeronautics and Astronautics, Inc. with permission.

In the context of the SD method for three-dimensional unstructured hexahedral grids, the present study addresses the implementation of a structural SGS model based on the scale similarity assumption,<sup>18</sup> namely, the WALE Similarity Mixed model (WSM) proposed by Lodato et al.<sup>19</sup> To the authors' knowledge, this represents the first implementation of a structural SGS model in a three-dimensional solver that uses the SD method. Moreover, the proposed implementation of a constrained discrete filter of arbitrary order for the SD method will be suitable for a broad class of numerical schemes based on the discontinuous finite element representation of the solution, such as the family of energy stable schemes that can be obtained within the unifying Flux Reconstruction (FR) framework.<sup>4,20–28</sup>

## II. Mathematical formulation

### A. The numerical scheme

In the present work, the Navier-Stokes equations are solved using the high-order unstructured SD method for spatial discretization. The formulation of the equations on hexahedral grids is similar to the formulation by Sun et al.,<sup>7</sup> which will be summarized below for completeness. After introducing the *bar* filter operator and the density-weighted Favre filter operator *tilde*, the unsteady compressible Navier-Stokes equations in conservative form are written as

$$\frac{\partial \bar{\mathbf{U}}}{\partial t} + \frac{\partial \bar{\mathbf{F}}^k}{\partial x_k} = \mathbf{0}, \quad (1)$$

where  $\bar{\mathbf{U}} = \left( \bar{\rho} \quad \bar{\rho}u_1 \quad \bar{\rho}u_2 \quad \bar{\rho}u_3 \quad \bar{\rho}e \right)^T$  is the vector of conservative variables, and  $\bar{\mathbf{F}}^k = \bar{\mathbf{F}}_I^k - \bar{\mathbf{D}}^k$  accounts for the inviscid and viscous flux vectors, which are defined as

$$\bar{\mathbf{F}}_I^k = \begin{pmatrix} \bar{\rho}u_k \\ \bar{\rho}u_1\tilde{u}_k + \delta_{1k}\bar{\varpi} \\ \bar{\rho}u_2\tilde{u}_k + \delta_{2k}\bar{\varpi} \\ \bar{\rho}u_3\tilde{u}_k + \delta_{3k}\bar{\varpi} \\ (\bar{\rho}e + \bar{\varpi})\tilde{u}_k \end{pmatrix}, \quad \bar{\mathbf{D}}^k = \begin{pmatrix} 0 \\ 2\bar{\mu}\tilde{A}_{1k} + \tau_{1k}^d \\ 2\bar{\mu}\tilde{A}_{2k} + \tau_{2k}^d \\ 2\bar{\mu}\tilde{A}_{3k} + \tau_{3k}^d \\ 2\bar{\mu}\tilde{u}_j\tilde{A}_{kj} + \frac{\bar{\mu}c_p}{Pr} \frac{\partial \tilde{\vartheta}}{\partial x_k} + q_k \end{pmatrix}, \quad (2)$$

where  $\rho$  is the fluid's density,  $u_k$  is the velocity vector,  $e$  is the total energy (internal + kinetic),  $\mu$  is the dynamic viscosity,  $A_{ij}$  is the deviator of the deformation tensor,  $c_p$  is the specific heat capacity at constant pressure and  $Pr$  is the Prandtl number. In particular,  $\bar{\varpi}$  and  $\tilde{\vartheta}$  are the filtered *macro-pressure* and *macro-temperature*,<sup>19,29</sup> these quantities being related by the usual equation of state, i.e.,  $\bar{\varpi} = \bar{\rho}R\tilde{\vartheta}$ .  $\tau_{ij}$  and  $q_k$  in Eq. (2) represent the usual unclosed SGS terms (note that the superscript 'd' refers to the deviatoric part of the relevant tensor).

To achieve an efficient implementation, all elements in the physical domain are transformed to a standard cubic element described by local coordinates  $\boldsymbol{\xi} = (\xi_1, \xi_2, \xi_3)$ , with  $\boldsymbol{\xi} \in [0 : 1]^3$ . The governing equations in the physical domain are then transferred into the computational domain, and they take the form

$$\frac{\partial \bar{\mathbf{U}}}{\partial t} + \frac{\partial \bar{\mathcal{F}}^k}{\partial \xi_k} = \mathbf{0}, \quad (3)$$

where

$$\bar{\mathbf{U}} = |\det(\mathbf{J})|\bar{\mathbf{U}} \quad \text{and} \quad \bar{\mathcal{F}}^k = |\det(\mathbf{J})| \frac{\partial \xi_k}{\partial x_j} \bar{\mathbf{F}}^j, \quad (4)$$

and  $\det(\mathbf{J})$  represents the determinant of the Jacobian matrix  $J_{ij} = \partial x_i / \partial \xi_j$ .

Within each standard element, two sets of points are defined, namely the solution points and the flux points, as schematically illustrated in figure 1 for a one-dimensional element. In order to construct a degree  $(N - 1)$  polynomial for each coordinate direction, solution at  $N$  points are required. These  $N$  points in 1D are chosen to be the Gauss-Legendre quadrature points, whereas the flux points were selected to be the Gauss-Legendre quadrature points of order  $N - 1$  plus the two end points 0 and 1. Using the  $N$  solution points and the  $N + 1$  flux points, polynomials of degree  $N - 1$  and  $N$ , respectively, can be built using Lagrange bases defined as

$$h_i(\xi) = \prod_{s=1, s \neq i}^N \left( \frac{\xi - \xi_s}{\xi_i - \xi_s} \right), \quad \text{and} \quad l_{i+1/2}(\xi) = \prod_{s=0, s \neq i}^N \left( \frac{\xi - \xi_{s+1/2}}{\xi_{i+1/2} - \xi_{s+1/2}} \right). \quad (5)$$

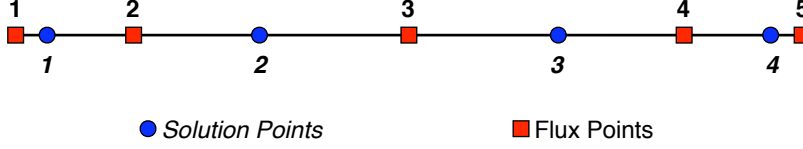


Figure 1. Schematic representation of the one dimensional distribution of solution and flux points within the SD element for  $N = 4$ .

The reconstructed solution for the conserved variables in the standard element is then obtained as the tensor product of the three one-dimensional polynomials,

$$\bar{U}(\boldsymbol{\xi}) = \sum_{k=1}^N \sum_{j=1}^N \sum_{i=1}^N \frac{\bar{u}_{i,j,k}}{|J_{i,j,k}|} h_i(\xi_1) h_j(\xi_2) h_k(\xi_3), \quad (6)$$

where  $i$ ,  $j$  and  $k$  are the indices of the solution points within each standard element. A similar reconstruction is adopted for the resolved fluxes  $\bar{\mathcal{F}}^k$ .

The reconstructed fluxes are only element-wise continuous, but discontinuous across cell interfaces. For the inviscid flux, a Riemann solver is employed to compute a common flux at cell interfaces to ensure conservation and stability. In the current implementation, the Roe solver<sup>30</sup> with entropy fix<sup>31</sup> was used. The left and right states here represent the solution on both sides of the shared edge flux point. The viscous flux is a function of both the conserved variables and their gradients, therefore, the solution gradients have to be calculated at the flux points. The average approach described by Sun et al.<sup>7</sup> is used to compute the viscous fluxes.

## B. LES modeling approach

In order to close the SGS terms a structural model based on the scale similarity assumption<sup>18,32,33</sup> is adopted. In the perspective of developing a similarity mixed formulation<sup>33-40</sup> with correct near-wall scaling, a WALE formulation<sup>16</sup> for the eddy-viscosity term was recently proposed by Lodato et al.:<sup>19</sup>

$$\tau_{ij}^d = 2\bar{\rho}\nu_{\text{sgs}}\tilde{A}_{ij} - \bar{\rho}(\widehat{u_i u_j} - \widehat{u_i} \widehat{u_j})^d, \quad (7)$$

$$q_k = \gamma\bar{\rho}\kappa_{\text{sgs}} \frac{\partial \tilde{e}_I}{\partial x_k} - \gamma\bar{\rho}(\widehat{e_I u_k} - \widehat{e_I} \widehat{u_k}), \quad (8)$$

where  $\tilde{e}_I$  is the resolved internal energy and the *hat* operator represents filtering at cutoff length  $\alpha\Delta$ , with  $\alpha \geq 1$  and sufficient localization in physical space.<sup>32</sup> the SGS kinematic viscosity,  $\nu_{\text{sgs}}$ , and thermal diffusivity,  $\kappa_{\text{sgs}}$ , are computed as<sup>16</sup>

$$\nu_{\text{sgs}} = C_w^2 \Delta^2 \frac{(\tilde{s}_{ij}^d \tilde{s}_{ij}^d)^{3/2}}{(\tilde{S}_{ij} \tilde{S}_{ij})^{5/2} + (\tilde{s}_{ij}^d \tilde{s}_{ij}^d)^{5/4}}, \quad \text{and} \quad \kappa_{\text{sgs}} = \frac{\nu_{\text{sgs}}}{Pr_{\text{sgs}}}, \quad (9)$$

where  $C_w = 0.5$ ,  $\Delta$  is a measure of the grid cutoff length scale, which is here evaluated following the same procedure suggested by Parsani et al.,<sup>15</sup> namely

$$\Delta(\boldsymbol{\xi}) \sim \left[ \frac{|\det(\mathbf{J}(\boldsymbol{\xi}))|}{N^3} \right]^{1/3}, \quad (10)$$

$\tilde{S}_{ij} = \frac{1}{2}(\partial \tilde{u}_i / \partial x_j + \partial \tilde{u}_j / \partial x_i)$  is the strain rate tensor of the resolved field and  $\tilde{s}_{ij}^d$  is the traceless symmetric part of the square of the resolved velocity gradient tensor  $\tilde{g}_{ij} = \partial \tilde{u}_i / \partial x_j$ . The sub-grid scale Prandtl number,  $Pr_{\text{sgs}}$ , is assumed constant and equal to 0.5.<sup>38,40</sup>

### C. Constrained discrete filters for the SD method

When using similarity mixed SGS models, such as the WSM model used in this study, explicit filtering represents a key ingredient to approximate sub-grid scale interactions. This is done by assuming similarity within a narrow band of frequencies in the vicinity of the cutoff frequency  $k_c$ . As already mentioned in section B, similarity is assumed between the SGS scales and the smallest resolved scales, which are evaluated as the difference between the filtered and the twice-filtered field. Hence, the explicit filter should be designed (a) to have sufficient localization in physical space; (b) to ensure a certain selected cutoff length-scale. For instance, the box filter in physical space is generally used due to its locality and easy of implementation.<sup>19,37</sup> Lodato et al.,<sup>19</sup> in particular, used a discrete approximation with cutoff length-scale  $\widehat{\Delta} = 4/3\Delta$  according to what was proposed by Akhavan et al.,<sup>33</sup> this filter width being an optimal size in order to sufficiently isolate the smallest resolved scales. In the present study, a slightly higher—yet providing sufficient localization in physical space—value of  $1.5\Delta$  is adopted.

In order to develop a mixed similarity formulation to be applied with the SD method, the above ideas need to be generalized in a way which is numerically consistent with the use of SD elements. In particular, since the SGS model terms are evaluated at the flux points, the filtered quantities needs to be evaluated at the same flux points starting from the discrete solution at the solution points. This can be achieved by filtering the solution at the solution points first, and then extrapolating the filtered quantities at the flux points using the same Lagrange polynomials used to reconstruct the fluxes (cf. Eq. (5)).

Considering for simplicity the one-dimensional SD element depicted schematically in figure 1, a particularly desirable feature in building discrete filters is that the filter stencil does not lie across elements. Moreover, the non-uniform spacing of the solution points should be taken into account. The above considerations lead to the particularly challenging task of designing asymmetric non-uniform discrete filters with a fixed cutoff length-scale.

For the SD element depicted in figure 1, the discrete filter for a generic quantity  $\phi$  is defined as<sup>41</sup>

$$\bar{\phi}_s = \sum_{i=1}^N w_i^s \phi_i, \quad (s = 1, \dots, N), \quad (11)$$

where the  $s$  index refers to a quantity at the  $N$  solution points. For the case of hexahedral elements as in the present study, the generalization to three dimensions follows immediately by tensor product of 1D filtering operators.

The spectral signature of the above discrete filter is characterized by its associated transfer function in Fourier space,<sup>42</sup> which is readily obtained as

$$\widehat{G}_s(k) = \sum_{i=1}^N w_i^s \exp(-j\beta_i^s k\Delta), \quad \text{with} \quad \beta_i^s = \frac{\xi_i - \xi_s}{\Delta}, \quad (12)$$

where  $k$  is the wavenumber and  $j = \sqrt{-1}$ ;  $\xi_s$  represents the location of the solution points, whereas  $\Delta = 1/N$  is assumed to be the actual resolution within the SD element (cf. Eq. (10)).

A possible strategy to build discrete filters can be devised by exploiting the resolution properties of polynomials of different order, thus performing the explicit filtering operation by applying the Restriction-Prolongation (RP) technique in each computational cell.<sup>10,43</sup> Based on Eq. (12), for instance, the real part of the Fourier transform of the discrete filters constructed using the Restriction-Prolongation (RP) technique<sup>10</sup> for  $N = 3$  and 4 is plotted in figure 2(a, b), where the Gaussian filter, with cutoff length equal to  $1.5\Delta$ , is also represented for reference. As it is immediately evident, the cutoff frequency, viz., the frequency at which  $\widehat{G}_s(k) \simeq 0.5$ , for each solution point is different and thus the overall effective cutoff frequency is unpredictable. Furthermore, for  $N = 4$ , the most asymmetric filters, i.e., those represented with solid lines, have a relatively pronounced over-shoot in the low frequency range, a feature which may lead to non-physical growth of energy.<sup>41</sup>

In order to overcome these problems, a Constrained Discrete (CD) filter satisfying a selected set of conditions, were developed for the SD method. The method used to derive these CD filters is based on the work of Vasilyev et al.<sup>41</sup> In particular, starting from Eq. (12), the  $N$  filter weights  $w_i^s$  for the  $s$ -th solution point can be determined by providing  $N$  constraints. More precisely, a first obvious condition is related to the preservation of a constant variable, namely  $\sum_{i=1}^N w_i^s = 1$ . Then, starting from the idea of building

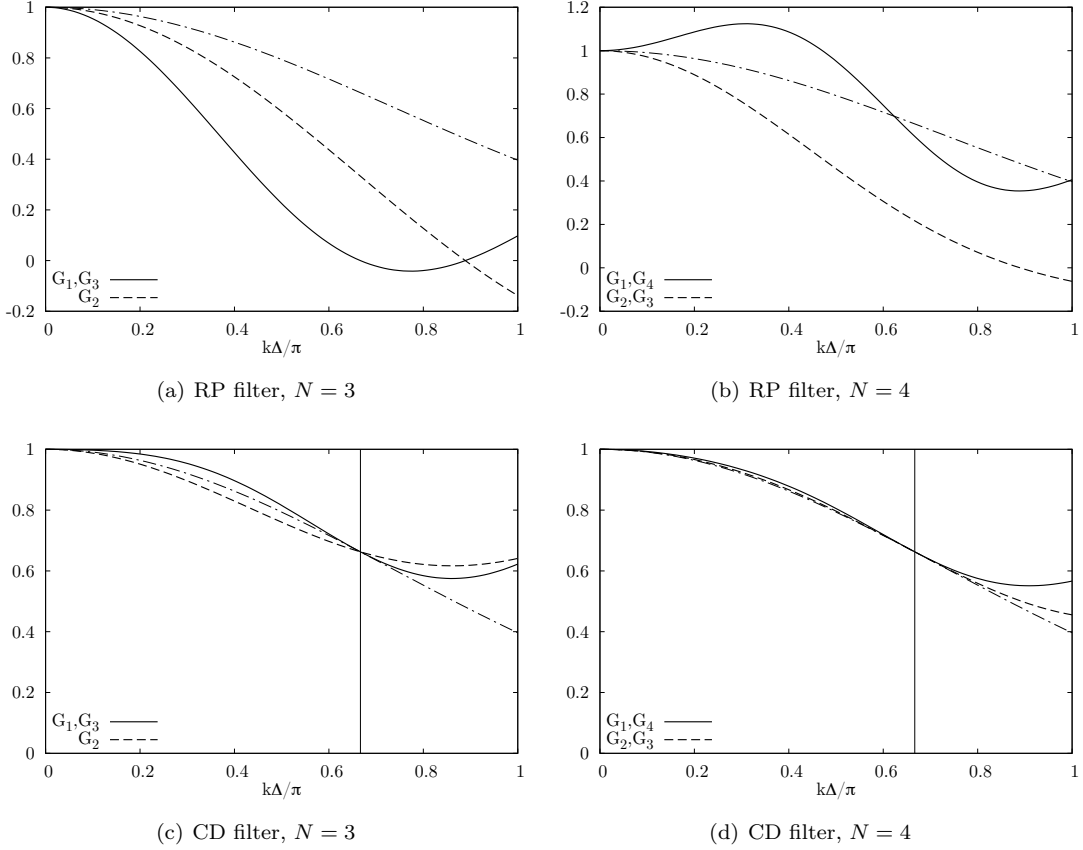


**Figure 2.** Real part of the transfer function  $\hat{G}(k\Delta/\pi)$  of RP<sup>10</sup> and CD filters for different SD discretization orders  $N$  (—, analytical Gaussian filter; vertical line: cutoff length-scale at  $1.5\Delta$ ).

filters whose kernels are as close as possible to that characterizing the Gaussian filter of width  $\Delta_c = \alpha\Delta$ , the condition

$$\text{Re}[\hat{G}_s(k_c)] = \sum_{i=1}^N w_i^s \cos(\beta_i^s k_c \Delta) = \exp\left(\frac{-\Delta_c^2 k_c^2}{4\gamma}\right)\Big|_{k=k_c} = \exp(-\pi^2/24), \quad (13)$$

is enforced, with  $k_c = \pi/\Delta_c$ , therefore constraining the relevant cutoff length-scale. The remaining conditions are obtained by constraining the discrete filter to have  $N - 2$  vanishing moments, thus achieving formal commutation with difference operators.<sup>41</sup>

The real part of the kernels of these CD filters for SD elements of order 3 and 4 are plotted in figure 2(c, d). As it can be observed, these CD filters approximate the reference filter much more accurately than the RP filters in the low frequency range, showing more pronounced deviations only at length-scales close to  $\Delta$  (i.e.  $k\Delta/\pi \rightarrow 1$ ). However, recalling that  $\Delta \sim O(1/N)$ , these small scales are not expected to play a significant role as they are supposedly not supported by the actual resolution of the SD element. The actual cutoff frequency is also more predictable throughout the SD element. Moreover, the over-shoots observed in the asymmetric filters constructed by the RP method, are now completely suppressed, hence a better numerical behavior in terms of stability is expected.

### III. Results and discussion

In this section, the results obtained with the actual implementation WSM model are presented. Computations on two different geometries are reported: (a) channel flow at Reynolds numbers of 180 and 395 (based on the friction velocity and channel half-width); (b) flow past a confined circular cylinder at Reynolds number 2580 (based on the upstream bulk velocity and cylinder diameter). For comparison, implicit LES

	$Re_\tau$	$Re_c$	$L_x \times L_y \times L_z$	$n_x \times n_y \times n_z$	$N$	DoF	$\Delta_x^+$	$\Delta_y^+$	$\Delta_z^+$
CHN1	180	3 440	$4\pi\delta \times 2\delta \times 2\pi\delta$	$15 \times 15 \times 15$	4	216 000	38	2.0–10	19
CHN2	180	3 440	$4\pi\delta \times 2\delta \times 2\pi\delta$	$12 \times 12 \times 12$	5	216 000	38	2.0–10	19
CHN3	395	8 106	$2\pi\delta \times 2\delta \times 1\pi\delta$	$16 \times 12 \times 12$	4	147 456	39	1.2–43	26
CHN4	395	8 106	$2\pi\delta \times 2\delta \times 1\pi\delta$	$13 \times 9 \times 9$	5	131 625	38	2.1–33	28

**Table 1. Grid size and resolution for channel flow computations (resolution is estimated as the element size divided by the number of solution points). DoF =  $(n_x \times n_y \times n_z) \times N^3$  is the total number of degrees of freedom.**

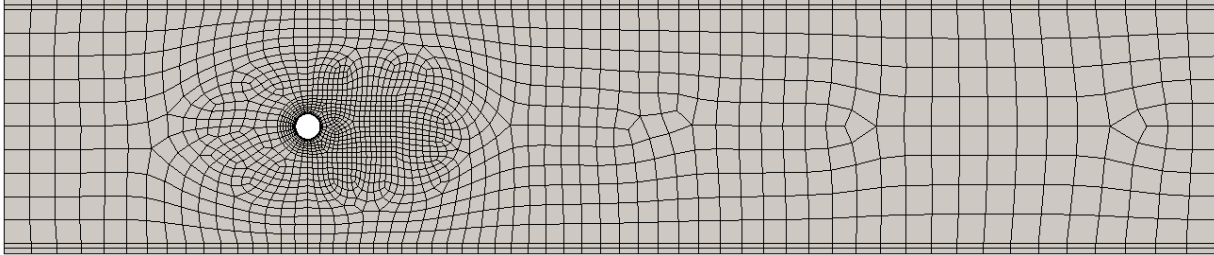


**Figure 3. Lateral view of the computational mesh for the cylinder in crossflow: 18 470 elements ( $5 \times 10^5$  DoF @  $N = 3$ );  $-12D$  to  $36D$  streamwise,  $-5D$  to  $5D$  vertical,  $-1.6D$  to  $1.6D$  spanwise; the cylinder, of diameter  $D$ , is centered at the origin.**

computations without the SGS model were performed as well.

### A. Turbulent channel flow

Two channel flow computations were performed at different orders ( $N = 4$  and  $5$ ) at  $Re_\tau = 180$  and  $395$  (based on the friction velocity  $u_\tau$  and channel half-width  $\delta$ ), and Mach number  $0.3$ . Grid dimensions and resolutions for the computations are summarized in table 1. Note that the resolution of the computation was estimated as the actual element size divided by the number of solution points used within the element; in a Finite Volume (FV) context, this is equivalent to assuming that each element is filled with  $N^3$  control volumes.

All the computations were performed with periodic boundary conditions in the streamwise and spanwise directions and no-slip isothermal walls were used on the top and bottom planes. In order to drive the flow, a source term  $\mathcal{S}$  was added to the  $x_1$  component of momentum. Given the compressible nature of the solver, in particular,  $\mathcal{S}$  was determined at each time-step in order to equilibrate the instantaneous resultant shear at the wall, plus a relaxation term toward the expected mass flow rate to accelerate convergence. For consistency, another source term, computed using the bulk velocity as  $u_b \mathcal{S}$ , was also added to the energy equation (isothermal walls were used to prevent the energy from increasing without bounds).

The computations were initialized with a uniform streamwise 4th-order velocity profile

$$u_1(\mathbf{x}) = \frac{15}{8} u_0 [1 - (x_2/\delta)^2]^2$$

( $u_0$  is the reference velocity) and a perturbed vertical velocity component.<sup>44,45</sup> After the flow field was fully developed and established, time averaging was performed for a period corresponding to about 20 flow-through times; further ensemble averaging in the streamwise and spanwise directions was also performed.

First- and second-order statistical moments are plotted in figures 4–6, where the the results from the explicit LES with the WSM model and the implicit LES are compared to the results from the Direct Numerical Simulations (DNS) performed by Moser et al.<sup>46</sup> Note that the extremely small density variation ( $\sim 1.4\%$  increase from centerline to the wall) did not make it necessary to use the Van Driest correction.<sup>47</sup>

The behavior of the WSM model in reproducing the statistical features of the flow is quite satisfactory for each test case. With regards to the mean velocity profiles, the slope of the log law is correctly represented, whereas its intercept is slightly overestimated with respect to the DNS value. The higher order computation gives results in better agreement with the DNS data, even if the DoF and spatial resolution are the same.

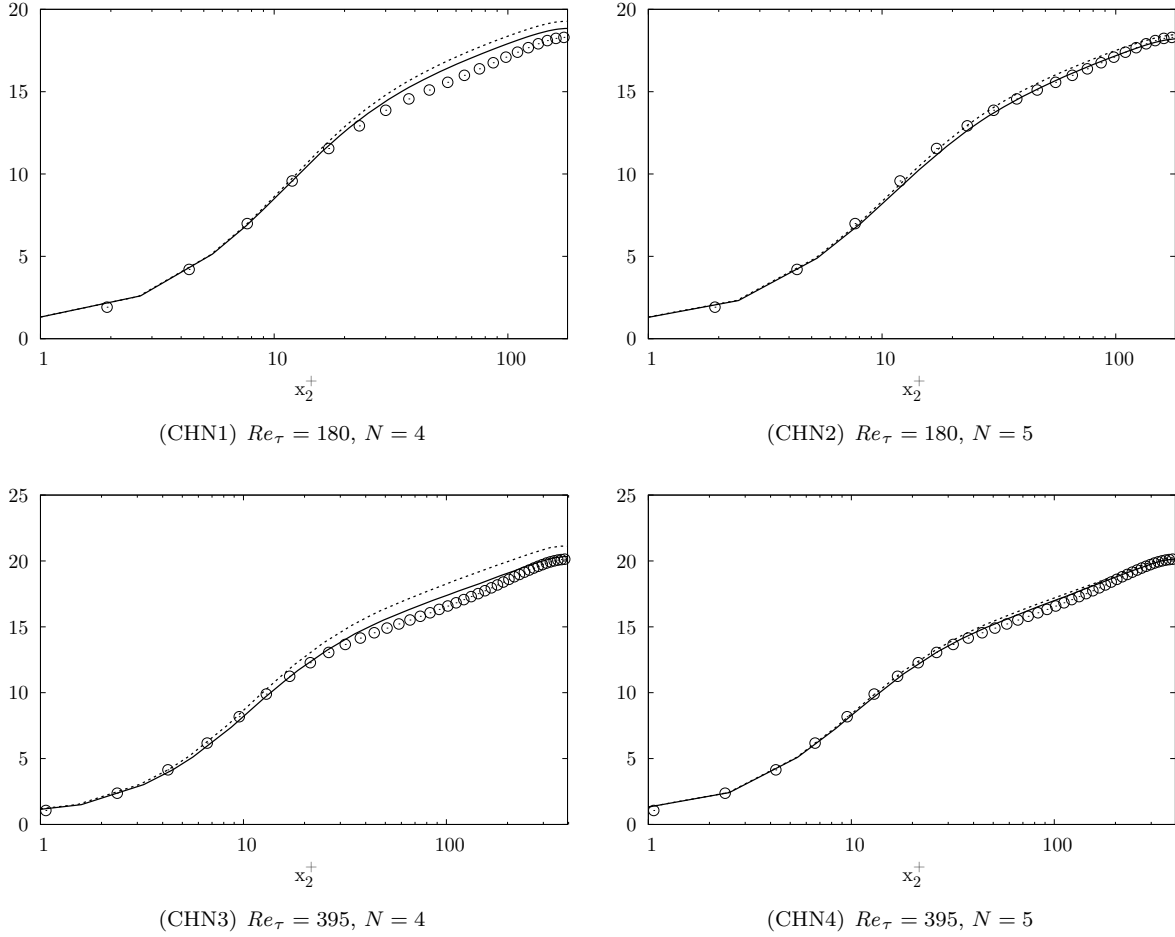


**Figure 4.** Mean streamwise velocity profile  $U^+$ : — , WSM model; ····· , no SGS model; ○ , DNS data.<sup>46</sup>

Overall, the use of the SGS model determines an improvement in the results obtained by implicit LES, which is more evident for the computations with four solution points per element. Reynolds stresses (cf. figure 5) are more sensitive to the use of the SGS model.

With regards to the root mean square (RMS) of the resolved velocity fluctuations, in particular, the profiles obtained with the use of the WSM model are in good agreement with the DNS data, regardless of the spatial discretization order, whereas the implicit LES shows some dependence to the order of the computation. The location and intensity of the peak of streamwise velocity fluctuation is correctly captured. Spanwise and vertical fluctuations tends to be slightly underestimated. Also shown in figures 5 and 6 for the case CHN3 is the curve obtained when the model term is computed using the RP filter. The results in this case show a marked oscillatory behavior with spurious peaks at the location of the element interfaces. This behavior is probably due to the over-shoots observed in the asymmetric filters constructed by the RP method for  $N = 4$  (cf. figure 2(b), solid line curve).

The resolved turbulent shear stresses from the LES are always below the DNS curves, whereas the results from implicit LES are much closer (cf. figure 6). Given the close connection between the mean streamwise velocity profile and the turbulent shear stress across the channel—the two quantities are strictly related through the steady Reynolds averaged  $x_1$  momentum equation—and given the good agreement observed for the former quantity, it is here argued that the actual global turbulent shear from LES, viz. resolved + SGS modeled contribution, is in good agreement with its DNS counterpart. This is readily confirmed for test cases CHN1 and CHN4 by collecting the mean SGS shear stress  $\langle \tau_{12} \rangle$  during the computation and by comparing the *exact* turbulent shear from DNS  $\langle \bar{u}'_1 \bar{u}'_2 \rangle$  with the approximate global (resolved + SGS) turbulent shear from LES, viz.  $\langle \bar{u}'_1 \bar{u}'_2 \rangle + \langle \tau_{12} \rangle$ .<sup>48</sup> As it can be observed in figure 6 (CHN1 and CHN4), the approximate global

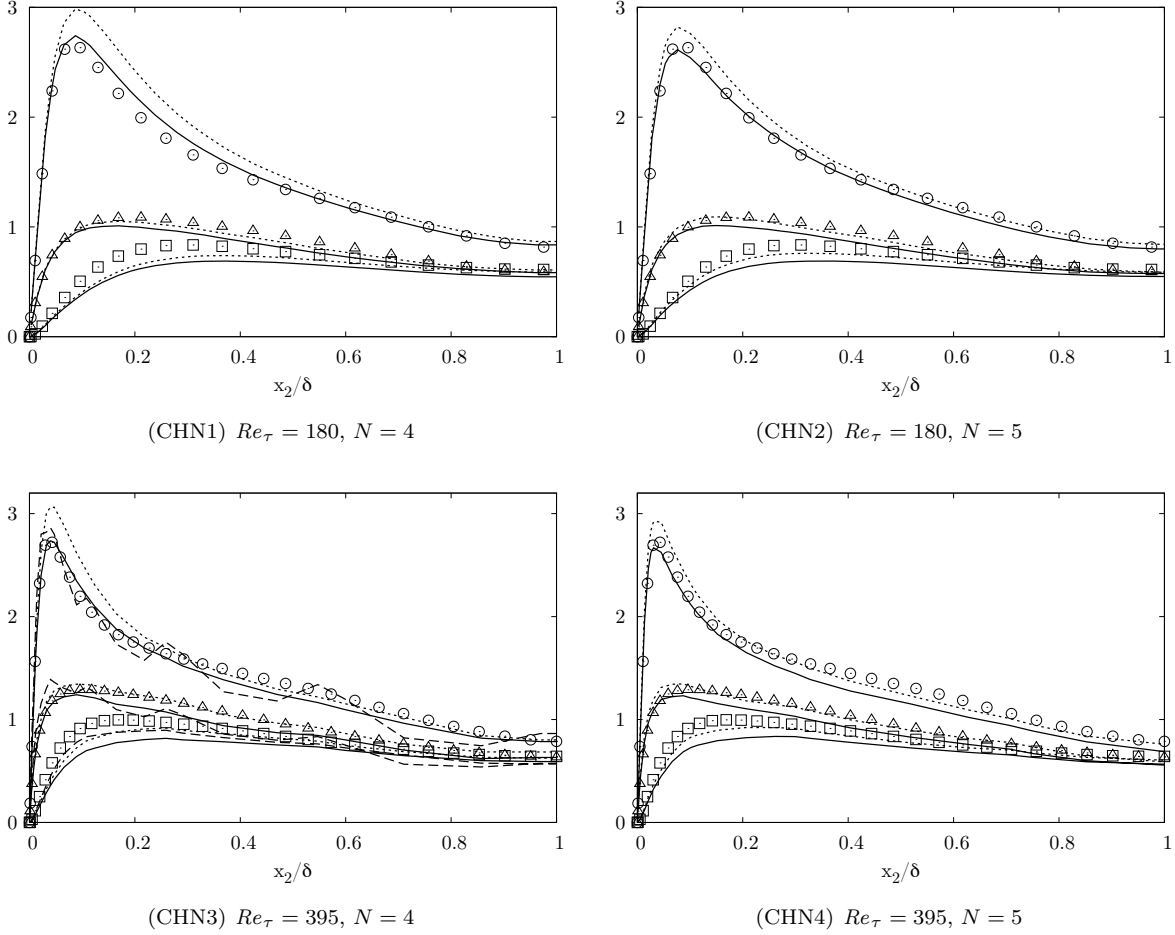


**Figure 5.** RMS of velocity fluctuations: —, WSM model (CD filter); - - - - , WSM model (RP filter); ·····, no SGS model; symbols, DNS data.<sup>46</sup>  $\circ$ ,  $u_{rms}^+$ ;  $\square$ ,  $v_{rms}^+$ ;  $\triangle$ ,  $w_{rms}^+$ .

turbulent shear matches almost perfectly the DNS data.

## B. Flow past a circular cylinder

The simulations, an implicit LES and an explicit LES with the WSM model and the new discrete filter, were performed at Reynolds and Mach numbers of 2580 and 0.25, respectively, based on the bulk velocity at the inlet  $U_b$  and the cylinder diameter  $D$ . The equations were integrated over an unstructured computational mesh of dimension  $48D \times 10D \times 3.2D$  ( $L \times H \times W$ ) with 18470 unstructured hexahedral elements, and  $N = 3$ . Therefore, the number of DoF was equal to 498690. Note that, compared to the resolution of the structured coarse mesh used by Mohammad et al.<sup>12</sup> for a similar LES computation, the resolution adopted here is about 5 times lower. Such a low resolution was used to assess the performances of the SGS model and the relevant discrete filters in a case in which the implicit LES is almost certainly expected to fail. The boundary conditions were periodic in the spanwise direction and no-slip adiabatic conditions were used on the top and bottom planes; the cylinder wall was set as no-slip adiabatic as well and the inflow/outflow conditions were imposed fixing the inlet density and velocity and the outlet pressure, respectively. After the flow field was fully developed and established, statistics were performed averaging in time for about 300 shedding periods, which, according to Parnaudeau et al.,<sup>51</sup> represents a long enough sample in order for statistics to be fully converged; in view of the statistical two-dimensionality of the flow field, further ensemble averaging in the spanwise direction was also performed. Results were compared against Particle Image Velocimetry (PIV) experimental measurements.<sup>49,50</sup>

First- and second-order statistical moments at different locations behind the cylinder, and along the

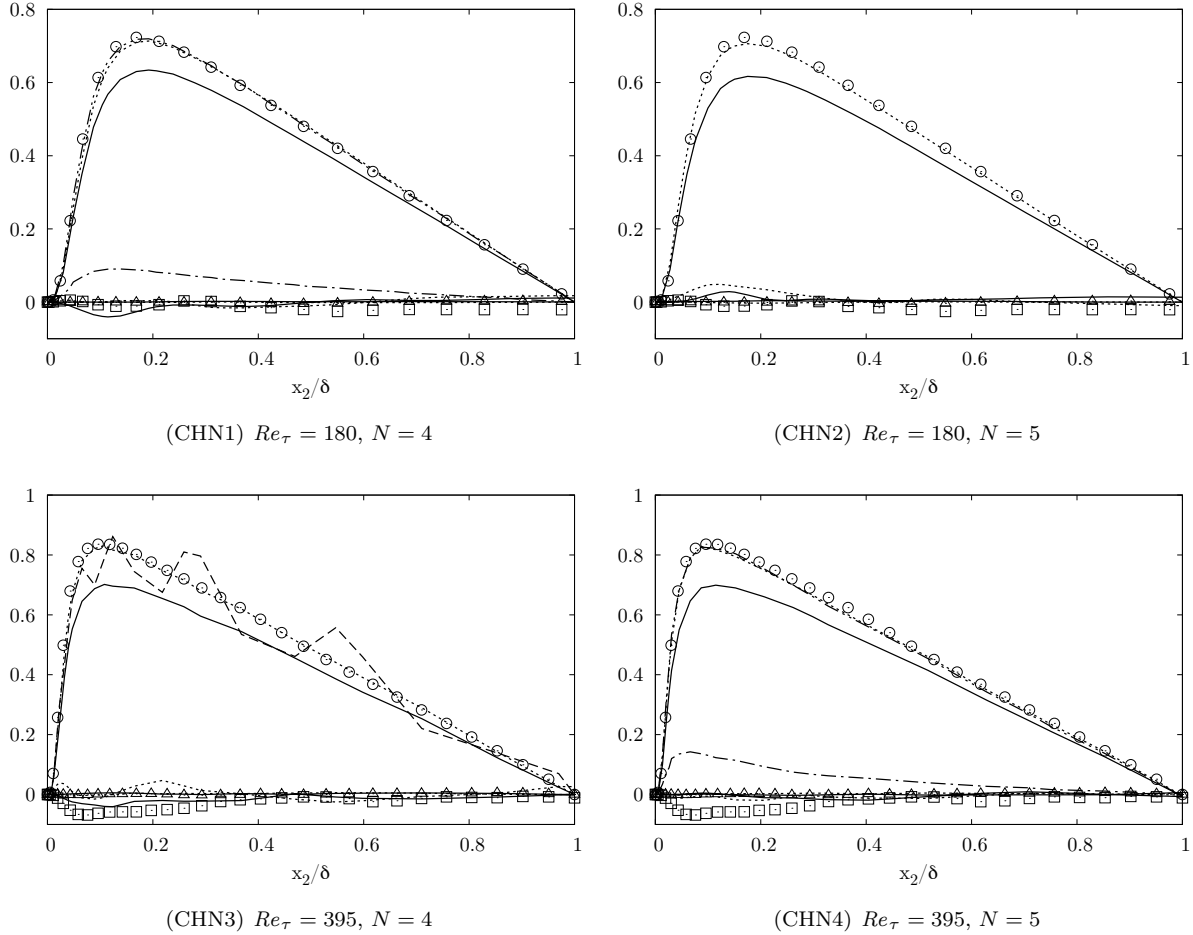


**Figure 6.** Reynolds shear stresses: —, WSM model (CD filter); ----, WSM model (RP filter); ·····, no SGS model; -·-·,  $\langle \tau_{12} \rangle$  from LES; - - - global shear stress from LES (resolved + SGS); symbols, DNS data.<sup>46</sup>  $\circ$ ,  $-\langle u^+ v^+ \rangle$ ;  $\square$ ,  $-\langle u^+ w^+ \rangle$ ;  $\triangle$ ,  $-\langle v^+ w^+ \rangle$ .

wake, are plotted in figures 7 and 8. Despite the extremely low resolution adopted, average profiles obtained using the SGS model are in very good agreement with the experimental data. The recirculation length, an extremely sensitive parameter for this kind of flow configuration, is well captured as well (cf. the mean velocity inversion point in figure 8). The computation without the SGS model, as expected, does not perform well. Significant deviations from the experimental data are observed, and the recirculation length is over predicted of about 20%.

With regards to the second-order statistical moments, results are not fully satisfactory even when the SGS model is used. Even though some improvement over the implicit LES is observed for  $x/D \geq 2$ , it is difficult to judge which computation is performing better. Grid resolution is clearly too low for the model used to be able to correctly reproduce also the Reynolds stresses. Further tests are under way using more suitable resolutions of  $1.2 \times 10^6$  and  $2.3 \times 10^6$  DoF (i.e.  $N = 4$  and 5, respectively).

#### IV. Concluding remarks

Overall, the performance of the actual WSM model implementation in conjunction with the SD method and the new discrete filters is extremely satisfactory. In both the flow configurations studied, statistical moments are generally improved when the SGS model is used. Depending on the grid resolution, the benefits resulting from using the SGS model are of different nature. First-order statistical moments are significantly improved, the improvement being especially evident in the case of relatively under-resolved LES

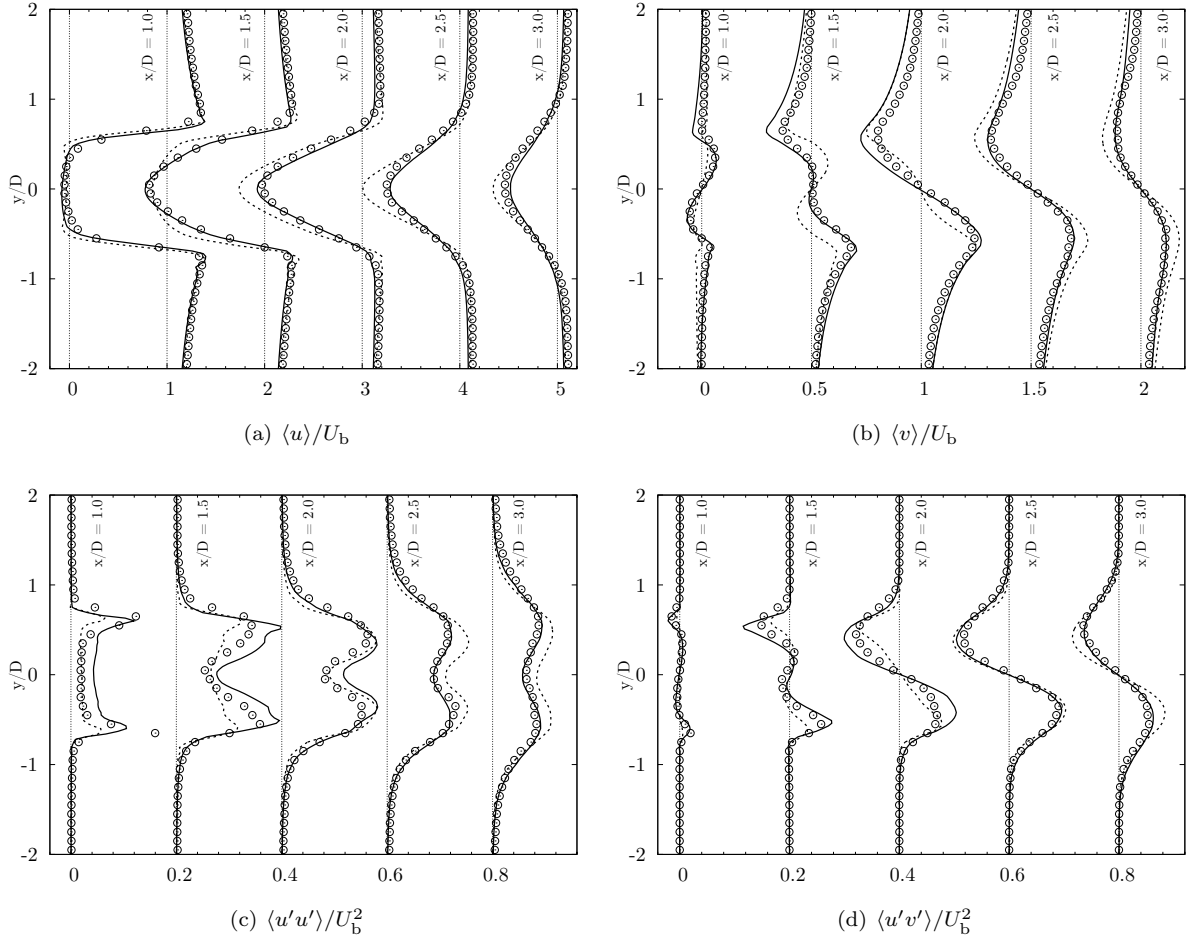


Figure 7. First- and second-order statistical moments of the resolved velocity field at different locations downstream of the cylinder: —, WSM model; ·····, no SGS model;  $\circ$ , experimental PIV measurements<sup>49,50</sup> (every two points represented). Light dotted lines represent the zero location of the shifted curves.

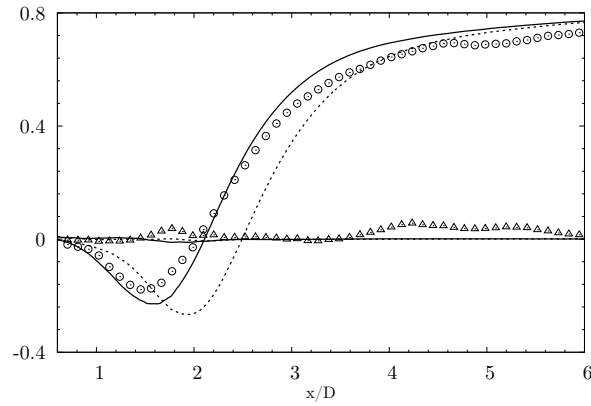


Figure 8. Streamwise and vertical average velocity measured along the wake of the cylinder at  $y/D = 0$ : —, WSM model; ·····, no SGS model; symbols ( $\circ$ , streamwise;  $\triangle$ , vertical), experimental PIV measurements<sup>49,50</sup> (every two points represented).

computations, where the implicit LES cannot be expected to give satisfactory results. More challenging is, of course, to reproduce second-order statistical moments which, in order to be correctly captured, still need

the grid to resolve enough turbulent kinetic energy. For sufficiently resolved computations, improvements in the Reynolds stresses were observed when the WSM model was turned on, whereas in the case of coarse LES computations, the improvements were more subtle.

The proposed constrained discrete filters of arbitrary order, in particular, proved to be numerically stable at any tested order (up to  $N = 7$  in other tests not included here) and allow a relatively straightforward implementation into high-order SD schemes (or any other discontinuous finite element numerical method) of any SGS model which relies upon the use of explicit filtering or dynamic procedures.<sup>52,53</sup> For the similarity mixed formulation used in the present study, in particular, existing filtering approaches based on solution projection over low-order polynomial bases proved to be inadequate, and keen to develop spurious numerical artifacts at the elements interfaces. In the tests performed, the newly developed discrete filters did not lead to any similar unexpected and unphysical behavior throughout the computational domain. Further development of wall modeling procedures and the unstructured nature of the high-order SD scheme will also allow relatively affordable high fidelity LES computations in complex geometries.

## References

- <sup>1</sup>Hesthaven, J. and Warburton, T., *Nodal discontinuous Galerkin methods: algorithms, analysis, and applications*, Springer Verlag, 2007.
- <sup>2</sup>Karniadakis, G. and Sherwin, S., *Spectral/hp element methods for CFD*, Oxford University Press, USA, 1999.
- <sup>3</sup>Kopriva, D. and Kolias, J., “A conservative staggered-grid Chebyshev multidomain method for compressible flows,” *J. Comput. Phys.*, Vol. 125, No. 1, 1996, pp. 244–261.
- <sup>4</sup>Huynh, H., “A Flux Reconstruction Approach to High-Order Schemes Including Discontinuous Galerkin Methods,” *AIAA P.*, Vol. 2007-4079, 2007, 18th AIAA Computational Fluid Dynamics Conference, Miami, FL, Jun. 25–28, 2007.
- <sup>5</sup>Liu, Y., Vinokur, M., and Wang, Z., “Spectral difference method for unstructured grids I: basic formulation,” *J. Comput. Phys.*, Vol. 216, No. 2, 2006, pp. 780–801.
- <sup>6</sup>May, G. and Jameson, A., “A spectral difference method for the Euler and Navier-Stokes equations on unstructured meshes,” *AIAA P.*, Vol. 2006-304, 2006, 44th AIAA Aerospace Sciences Meeting, Reno, NV, Jan. 9–12, 2006.
- <sup>7</sup>Sun, Y., Wang, Z., and Liu, Y., “High-order multidomain spectral difference method for the Navier-Stokes equations on unstructured hexahedral grids,” *Commun. Comput. Phys.*, Vol. 2, No. 2, 2007, pp. 310–333.
- <sup>8</sup>Wang, Z., Liu, Y., May, G., and Jameson, A., “Spectral difference method for unstructured grids II: Extension to the Euler equations,” *J. Sci. Comput.*, Vol. 32, No. 1, 2007, pp. 45–71.
- <sup>9</sup>Liang, C., Jameson, A., and Wang, Z., “Spectral difference method for compressible flow on unstructured grids with mixed elements,” *J. Comput. Phys.*, Vol. 228, No. 8, 2009, pp. 2847–2858.
- <sup>10</sup>Premasuthan, S., Liang, C., and Jameson, A., “A Spectral Difference method for viscous compressible flows with shocks,” *AIAA P.*, Vol. 2009-3785, 2009, 19th AIAA Computational Fluid Dynamics, San Antonio, Texas, Jun. 22–25, 2009, 16 p.
- <sup>11</sup>Liang, C., Premasuthan, S., Jameson, A., and Wang, Z., “Large eddy simulation of compressible turbulent channel flow with spectral difference method,” *AIAA P.*, Vol. 2009-402, 2009, 47th AIAA Aerospace Sciences Meeting Including The New Horizons Forum and Aerospace Exposition, Orlando, FL, Jan. 5–8, 2009, 15 p.
- <sup>12</sup>Mohammad, A., Wang, Z., and Liang, C., “Large Eddy Simulation of Flow over a Cylinder Using High-Order Spectral Difference Method,” *Adv. Appl. Math. Mech.*, Vol. 2, No. 4, 2010, pp. 451–466.
- <sup>13</sup>Ou, K., Liang, C., Premasuthan, S., and Jameson, A., “High-Order Spectral Difference Simulation of Laminar Compressible Flow Over Two Counter-Rotating Cylinders,” *AIAA P.*, Vol. 2009-3956, 2009, 27th AIAA Applied Aerodynamics Conference, San Antonio, TX, Jun. 22–25, 2009.
- <sup>14</sup>Castonguay, P., Liang, C., and Jameson, A., “Simulation of Transitional Flow over Airfoils using the Spectral Difference Method,” *AIAA P.*, Vol. 2010-4626, 2010.
- <sup>15</sup>Parsani, M., Ghorbaniasl, G., Lacor, C., and Turkel, E., “An implicit high-order spectral difference approach for large eddy simulation,” *J. Comput. Phys.*, Vol. 229, No. 14, 2010, pp. 5373–5393.
- <sup>16</sup>Nicoud, F. and Ducros, F., “Subgrid-Scale Stress Modelling Based on the Square of the Velocity Gradient Tensor,” *Flow Turbul. Combust.*, Vol. 62, No. 3, Sept. 1999, pp. 183–200.
- <sup>17</sup>Parsani, M., Ghorbaniasl, G., and Lacor, C., “Validation and application of an high-order spectral difference method for flow induced noise simulation,” *J. Comput. Acoust.*, Vol. 19, No. 3, 2011, pp. 241–268.
- <sup>18</sup>Bardina, J., Ferziger, J., and Reynolds, W., “Improved subgrid-scale models for large-eddy simulation,” *AIAA P.*, Vol. 1980-1357, July 1980, Fluid and Plasma Dynamics Conference, 13th, Snowmass, CO, Jul. 14–16, 1980, 10 p.
- <sup>19</sup>Lodato, G., Vervisch, L., and Domingo, P., “A Compressible Wall-Adapting Similarity Mixed Model for Large-Eddy Simulation of the Impinging Round Jet,” *Phys. Fluids*, Vol. 21, No. 3, 2009, pp. 035102.
- <sup>20</sup>Huynh, H., “A Reconstruction Approach to High-Order Schemes Including Discontinuous Galerkin for Diffusion,” *AIAA P.*, Vol. 2009-403, 2009, 47th AIAA Aerospace Sciences Meeting, Orlando, FL, Jan. 5–8, 2009.
- <sup>21</sup>Jameson, A., “A Proof of the Stability of the Spectral Difference Method for All Orders of Accuracy,” *J. Sci. Comput.*, Vol. 45, No. 1, 2010, pp. 348–358.
- <sup>22</sup>Jameson, A., “Advances in Bringing High-Order Methods to Practical Applications in Computational Fluid Dynamics,” *AIAA P.*, Vol. 2011-3226, 2011, 20th AIAA Computational Fluid Dynamics Conference, Honolulu, Hawaii, Jun. 27–30, 2011.
- <sup>23</sup>Jameson, A., Vincent, P., and Castonguay, P., “On the non-linear stability of flux reconstruction schemes,” *J. Sci. Comput.*, Vol. 50, No. 2, 2012, pp. 434–445.

- <sup>24</sup>Vincent, P., Castonguay, P., and Jameson, A., “A New Class of High-Order Energy Stable Flux Reconstruction Schemes,” *J. Sci. Comput.*, Vol. 47, No. 1, 2010, pp. 1–23.
- <sup>25</sup>Vincent, P., Castonguay, P., and Jameson, A., “Insights from von Neumann analysis of high-order flux reconstruction schemes,” *J. Comput. Phys.*, Vol. 230, No. 22, 2011, pp. 8134–8154.
- <sup>26</sup>Vincent, P. and Jameson, A., “Facilitating the adoption of unstructured high-order methods amongst a wider community of fluid dynamicists,” *Math. Model. Nat. Phenom.*, Vol. 6, No. 3, 2011, pp. 97–140.
- <sup>27</sup>Williams, D., Castonguay, P., Vincent, P., and Jameson, A., “An Extension of Energy Stable Flux Reconstruction to Unsteady, Non-linear, Viscous Problems on Mixed Grids,” *AIAA P.*, Vol. 2011-3405, 2011, pp. 37, 20th AIAA Computational Fluid Dynamics Conference, Honolulu, Hawaii, Jun. 27–30, 2011.
- <sup>28</sup>Castonguay, P., Vincent, P., and Jameson, A., “A New Class of High-Order Energy Stable Flux Reconstruction Schemes for Triangular Elements,” *J. Sci. Comput.*, 2011, pp. 1–33.
- <sup>29</sup>Lesieur, M., Métais, O., and Comte, P., *Large-Eddy Simulations of Turbulence*, Cambridge University Press, 2005.
- <sup>30</sup>Roe, P., “Approximate Riemann Solvers, Parameter Vectors, and Difference Schemes,” *J. Comput. Phys.*, Vol. 43, 1981, pp. 357–372.
- <sup>31</sup>Harten, A., “High resolution schemes for hyperbolic conservation laws,” *J. Comput. Phys.*, Vol. 49, No. 3, 1983, pp. 357–393.
- <sup>32</sup>Liu, S., Meneveau, C., and Katz, J., “On the properties of similarity subgrid-scale models as deduced from measurements in a turbulent jet,” *J. Fluid Mech.*, Vol. 275, 1994, pp. 83–119.
- <sup>33</sup>Akhavan, R., Ansari, A., Kang, S., and Mangiavacchi, N., “Subgrid-scale interactions in a numerically simulated planar turbulent jet and implications for modeling,” *J. Fluid Mech.*, Vol. 408, 2000, pp. 83–120.
- <sup>34</sup>Salveti, M. and Banerjee, S., “A priori tests of a new dynamic subgrid-scale model for finite-difference large-eddy simulations,” *Phys. Fluids*, Vol. 7, No. 11, Nov. 1995, pp. 2831–2847.
- <sup>35</sup>Anderson, R. and Meneveau, C., “Effects of the Similarity Model in Finite-Difference LES of Isotropic Turbulence Using a Lagrangian Dynamic Mixed Model,” *Flow Turbul. Combust.*, Vol. 62, No. 3, 1999, pp. 201–225.
- <sup>36</sup>Zang, T., Dahlburg, R., and Dahlburg, J., “Direct and large-eddy simulations of three-dimensional compressible Navier-Stokes turbulence,” *Phys. Fluids A-Fluid*, Vol. 4, No. 1, Jan. 1992, pp. 127–140.
- <sup>37</sup>Zang, Y., Street, R. L., and Koseff, J. R., “A dynamic mixed subgrid-scale model and its application to turbulent recirculating flows,” *Phys. Fluids A-Fluid*, Vol. 5, No. 12, Dec. 1993, pp. 3186–3196.
- <sup>38</sup>Erlebacher, G., Hussaini, M., Speziale, C., and Zang, T., “Toward the large-eddy simulation of compressible turbulent flows,” *J. Fluid Mech.*, Vol. 238, 1992, pp. 155–185.
- <sup>39</sup>Speziale, C., “Galilean invariance of subgrid-scale stress models in the large-eddy simulation of turbulence,” *J. Fluid Mech.*, Vol. 156, 1985, pp. 55–62.
- <sup>40</sup>Speziale, C., Erlebacher, G., Zang, T., and Hussaini, M., “The subgrid-scale modeling of compressible turbulence,” *Phys. Fluids*, Vol. 31, No. 4, April 1988, pp. 940–942.
- <sup>41</sup>Vasilyev, O., Lund, T., and Moin, P., “A General Class of Commutative Filters for LES in Complex Geometries,” *J. Comput. Phys.*, Vol. 146, No. 1, 1998, pp. 82–104.
- <sup>42</sup>Berland, J., Bogey, C., Marsden, O., and Bailly, C., “High-order, low dispersive and low dissipative explicit schemes for multiple-scale and boundary problems,” *J. Comput. Phys.*, Vol. 224, No. 2, 2007, pp. 637–662.
- <sup>43</sup>Blackburn, H. and Schmidt, S., “Spectral element filtering techniques for large eddy simulation with dynamic estimation,” *J. Comput. Phys.*, Vol. 186, No. 2, 2003, pp. 610–629.
- <sup>44</sup>Andersson, P., Brandt, L., Bottaro, A., and Henningson, D., “On the breakdown of boundary layer streaks,” *J. Fluid Mech.*, Vol. 428, No. 1, 2001, pp. 29–60.
- <sup>45</sup>Rossi, R., “Direct numerical simulation of scalar transport using unstructured finite-volume schemes,” *J. Comput. Phys.*, Vol. 228, No. 5, 2009, pp. 1639–1657.
- <sup>46</sup>Moser, R., Kim, J., and Mansour, N., “Direct numerical simulation of turbulent channel flow up to  $Re_\tau = 590$ ,” *Phys. Fluids*, Vol. 11, No. 4, April 1999, pp. 943–945.
- <sup>47</sup>Foysi, H., Sarkar, S., and Friedrich, R., “Compressibility effects and turbulence scalings in supersonic channel flow,” *J. Fluid Mech.*, Vol. 509, No. 1, 2004, pp. 207–216.
- <sup>48</sup>Sagaut, P., *Large Eddy Simulation for Incompressible Flows: An Introduction*, Springer-Verlag Berlin Heidelberg, 2nd ed., 2001.
- <sup>49</sup>Konstantinidis, E., Balabani, S., and Yianneskis, M., “The effect of flow perturbations on the near wake characteristics of a circular cylinder,” *J. Fluid Struct.*, Vol. 18, No. 3-4, 2003, pp. 367–386.
- <sup>50</sup>Konstantinidis, E., Balabani, S., and Yianneskis, M., “Conditional averaging of PIV plane wake data using a cross-correlation approach,” *Exp. Fluids*, Vol. 39, No. 1, 2005, pp. 38–47.
- <sup>51</sup>Parnaudeau, P., Carlier, J., Heitz, D., and Lamballais, E., “Experimental and numerical studies of the flow over a circular cylinder at Reynolds number 3900,” *Phys. Fluids*, Vol. 20, 2008, pp. 085101.
- <sup>52</sup>Germano, M., Piomelli, U., Moin, P., and Cabot, W., “A dynamic subgrid-scale eddy viscosity model,” *Phys. Fluids A-Fluid*, Vol. 3, No. 7, July 1991, pp. 1760–1765.
- <sup>53</sup>Moin, P., Squires, K., Cabot, W., and Lee, S., “A dynamic subgrid-scale model for compressible turbulence and scalar transport,” *Phys. Fluids A-Fluid*, Vol. 3, No. 11, Nov. 1991, pp. 2746–2757.